Ag/Ag_3PO_4-doped $BiPO_4$ heterostructures and their photocatalytic applications under visible light irradiation

Yen-Jui Chen[a], Po-Jen Tseng[a], Chi-Shun Tseng[a], Chang-Wei Huang[a], Tsunghsueh Wu[b], Mei-Yao Wu[c], and Yang-Wei Lin[a,*]

[a] Department of Chemistry, National Changhua University of Education, Changhua City, Taiwan
[b]Department of Chemistry, University of Wisconsin-Platteville, Platteville, USA
[c]Research Centre for Traditional Chinese Medicine, Department of Medical Research, China Medical University Hospital, Taichung City, Taiwan
* Address correspondence to the authors for E-mail: linywjerry@cc.ncue.edu.tw

ABSTRACT

Ag/Ag_3PO_4-doped $BiPO_4$ ($Ag/Ag_3PO_4/BiPO_4$) heterostructures were synthesized by the hydrothermal method combined with the sonochemical process. Transmission electron microscopy and UV–Vis diffuse reflectance spectroscopy were used to characterize the heterostructures. The morphologies and optical properties of the heterostructures were determined to be drastically different from those of $BiPO_4$. $Ag/Ag_3PO_4/BiPO_4$ was used in the photocatalytic degradation of a dyestuff (methylene blue) and the disinfection of pathogens (*Escherichia coli*) under visible light (λ > 420 nm) irradiation, and it displayed considerably higher photocatalytic activity (>99% degradation and >99% disinfection within 20 min) than did pure $BiPO_4$. This enhanced photocatalytic activity of the $Ag/Ag_3PO_4/BiPO_4$ heterostructure can be attributed to the high separation efficiency and low recombination rate of photogenerated electron–hole pairs, as well as the Ag^+ ions release under visible light irradiation.

Keywords: $BiPO_4$, Ag/Ag_3PO_4-doped $BiPO_4$, visible light, degradation, disinfection

1 INTRODUCTION

The development of new methods to treat water pollution caused by organic dyestuffs and pathogens has been attracting growing interest [1-4]. In recent years, efforts have focused on the use of semiconductor-based photocatalysts for water treatment because of their ability to degrade organic dyestuffs and pathogens under light irradiation [5].

For example, $BiPO_4$ nanoparticles were found to exhibit high photocatalytic activity for organic dyestuff decomposition, because the nonmetal oxyacid PO_4^{3-} can effectively promote the separation of photogenerated electrons and holes [6, 7]. Similar to TiO_2, $BiPO_4$ has a wide band gap, and its photocatalytic activity under visible light irradiation is thus limited. One strategy employed to extend the absorbance of $BiPO_4$ to the visible light region is to combine it with another semiconductor or a metal [8, 9]. Noble metals such as Ag, and Au have attracted considerable attention because of their ability to enhance the separation efficiency of photogenerated electron–hole pairs [10-12]. A coprecipitation hydrothermal method was used to prepare a p–n junction $Ag_3PO_4/BiPO_4$ heterostructure, which had enhanced photocatalytic activity due to the highly efficient separation of photogenerated electrons and holes by the $Ag_3PO_4/BiPO_4$ heterojunction [13]. However, this heterostructure was unstable under light illumination, because it was easily deteriorated by the photogenerated electrons [14].

Herein, a systematic study of $Ag/Ag_3PO_4/BiPO_4$ preparation under hydrothermal conditions combined with the sonochemical procedure is presented for the first time. The photocatalytic degradation and antibacterial activity of the prepared $Ag/Ag_3PO_4/BiPO_4$ heterostructures were assessed according to their ability to degrade MB and to disinfect *Escherichia coli* (*E. coli*) under visible light irradiation.

2 EXPERIMENTAL

2.1 Preparation

The $BiPO_4$ photocatalyst was prepared using a previously reported method [15]. The Ag/Ag_3PO_4-loaded $BiPO_4$ ($Ag/Ag_3PO_4/BiPO_4$) was synthesized as follows: Pure $BiPO_4$ powder (0.300 g) was added to 10 mL of deionized water containing an appropriate amount of $AgNO_3$ (0.075 g). The mixture was exposed to high-intensity ultrasonic irradiation under ambient air. Ultrasonic irradiation was accomplished with a high-intensity ultrasonic probe (Misonix, Inc., USA, XL-2020, 20 kHz, 600 W) immersed directly into the solution. The total reaction time was 15 min. The subsequently formed yellow $Ag/Ag_3PO_4/BiPO_4$ powder were collected and washed three times with deionized water and ethanol, and then dried in a desiccator at 50 °C for 8 h.

2.2 Characterization

The morphologies of the prepared photocatalysts were observed using a JEOL-1200EX II TEM (JEOL) at an accelerating voltage of 200 kV. Diffuse reflectance spectra

(DRS) were produced by an Evolution 2000 UV–Vis spectrometer (Thermo Fisher) using $BaSO_4$ as the reference. PL spectra were produced using a Varian Cary Eclipse fluorescence spectrometer (Varian).

2.3 Photocatalytic degradation activity

$BiPO_4$ and $Ag/Ag_3PO_4/BiPO_4$ were used to degrade MB under UV (253.9 nm, 15 W) and visible light (>420.0 nm, 150 W) irradiation, respectively, and their photocatalytic activity was evaluated. The photocatalyst (0.2 g) was added to an aqueous solution containing MB (5 mg/L in 50 mL of solution) in a beaker at room temperature. Before light irradiation, the solution was stirred for 30 min in the dark to ensure an adsorption–desorption equilibrium. The solution was then irradiated with constant magnetic stirring. At given time intervals, 3 mL of the suspension was sampled and centrifuged to remove the powder catalyst. The concentration of MB during degradation was monitored through colorimetry using a Synergy H1 Hybrid Multi-Mode Microplate Reader (Biotek Instruments). All of the measurements were carried out at room temperature.

2.4 Photocatalytic antibacterial activity

E. coli was used as a gram-negative bacterial mode to evaluate the antibacterial activity of $BiPO_4$ and $Ag/Ag_3PO_4/BiPO_4$. All glasses and materials were sterilized at 110 °C for 20 min in an autoclave. The bacterial cells were cultured in a Luria-Bertani (LB) medium at 37 °C. The cells were then separated by centrifugation, washed, and re-suspended in the LB medium with the cell concentration maintained at approximately 10^8 cfu/mL. During each antibacterial test, 50 mL of bacterial suspension added to 5 mg of solid photocatalyst was continuously stirred under both dark and light irradiation conditions. To evaluate the disinfection process, 100 μL of the suspension was collected at certain time intervals, then diluted to 10^3 cfu/mL by medium and cultured on a nutrition agar for 24 h at 37 °C . The number of cells was counted according to colonies formed on the plate. At the end of each run, the concentration of silver ions in the solution was measured by an atomic absorption spectrophotometer (GBC scientific equipment, Braeside, Australia).

3 RESULTS AND DISCUSSION

3.1 Morphology

Figure 1 depicts TEM images of $BiPO_4$ and $Ag/Ag_3PO_4/BiPO_4$, clearly revealing differences in the morphology and size of the as-prepared photocatalysts. $BiPO_4$ was composed of rod-like structures with a diameter and length of 90 ± 10 and 1500 ± 340 nm, respectively (Figure 1). $Ag/Ag_3PO_4/BiPO_4$, which was prepared by mixing 0.300 g of $BiPO_4$ with 0.075 g of $AgNO_3$ through an impregnation procedure, was composed of irregular short rod-like heterostructures with a diameter and length of 150 ± 100 and 970 ± 550 nm, respectively (Figure 1B). High resolution TEM (HRTEM) measurements were performed to further analyze the structure of $Ag/Ag_3PO_4/BiPO_4$, Both Ag/Ag_3PO_4 and $BiPO_4$ could be clearly observed (Figure 1C) [16]. Ag nanoparticles with an average diameter of 17 ± 7 nm were deposited on the $BiPO_4$ surface, according to the HRTEM image of $Ag/Ag_3PO_4/BiPO_4$ (Figure 1D). This distinctive feature—Ag nanoparticles doped on the $BiPO_4$ surface—confers high photocatalytic activity on the $Ag/Ag_3PO_4/BiPO_4$ heterostructures, as discussed subsequently.

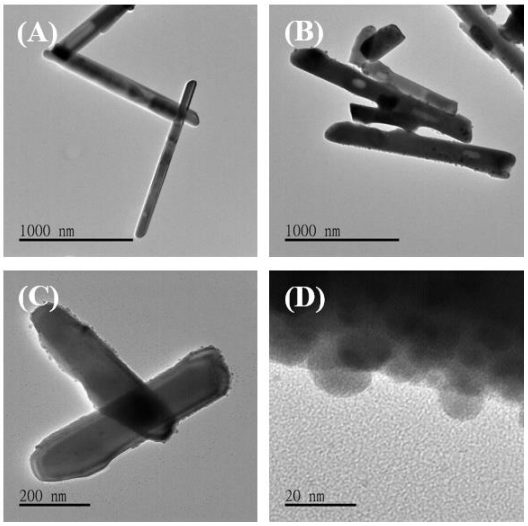

Figure 1. TEM and HRTEM images of (A) $BiPO_4$ and (B–D) $Ag/Ag_3PO_4/BiPO_4$.

3.2 DRS

Figure 2 illustrates the UV–Vis diffuse reflectance spectra (UV-DRS) of $BiPO_4$ and $Ag/Ag_3PO_4/BiPO_4$. Clearly, the white $BiPO_4$ samples absorbed only UV light, whereas the yellow $Ag/Ag_3PO_4/BiPO_4$ samples absorbed both UV and visible light. The Ag nanoparticles exhibited surface plasmon extinction bands centered at 450 nm, causing the yellow color of the $Ag/Ag_3PO_4/BiPO_4$ powders. The square root of the absorption coefficient was linearly correlated with energy, signifying that the absorption edges of $BiPO_4$ and $Ag/Ag_3PO_4/BiPO_4$ were due to indirect transitions (Figure 2B). The energy bandgaps of the prepared heterostructures were estimated from the intercept of the curve tangent with the x-axis on their UV-DRS plots. The estimated bandgap of the as-synthesized $BiPO_4$ sample was approximately 4.38 eV. Interestingly, unlike $BiPO_4$ products, $Ag/Ag_3PO_4/BiPO_4$ heterostructure exhibited two band gaps of 4.18 and 2.33 eV. The first one is intrinsic of $BiPO_4$, being similar to those of $BiPO_4$ samples. The band gap of 2.33 eV could be ascribed to the Ag_3PO_4 samples. This difference in bandgap may have created different degrees of separation between the photogenerated electrons

and holes and the heterostructures, which in turn may have caused the differences in photocatalytic activity.

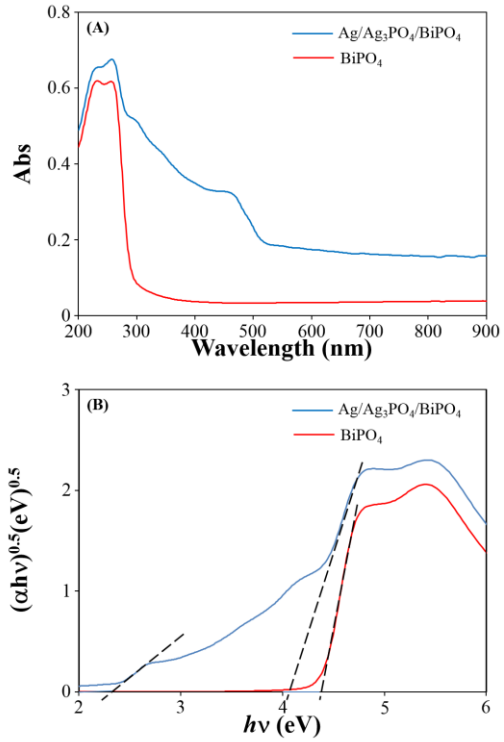

Figure 2. (A) Absorption spectra and (B) plots of $(Ah\nu)^{0.5}$ versus hν of $BiPO_4$ and $Ag/Ag_3PO_4/BiPO_4$.

3.3 Photocatalytic degradation activity

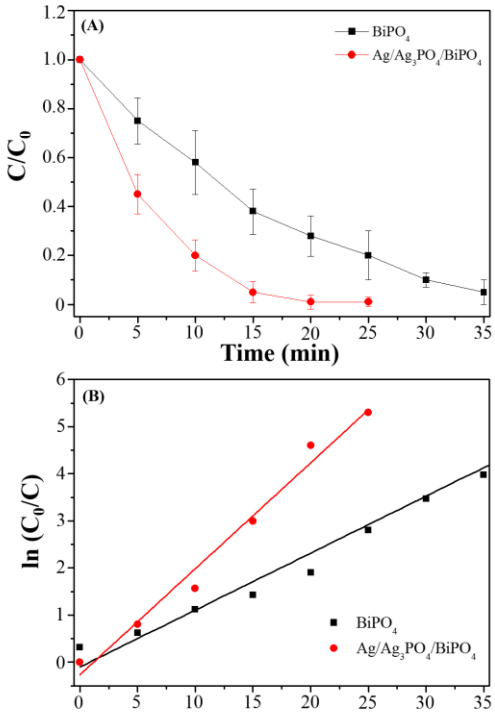

Figure 3. (A) Reduction of MB concentration C/C_0 with time and (B) corresponding rate constants of MB degradation by $BiPO_4$ under UV and $Ag/Ag_3PO_4/BiPO_4$ under visible light.

The photocatalytic performance of $BiPO_4$ and $Ag/Ag_3PO_4/BiPO_4$ during MB degradation under UV and visible light irradiation was evaluated. Figure 3A presents the change in MB concentration (C/C_0, where C_0 represents initial concentration and C represents concentration at time t) with irradiation time when each catalyst was used. To assess whether the as-prepared samples were active photocatalysts, a control experiment of direct MB photolysis without any photocatalyst was also performed under the same conditions, and this confirmed that the MB concentration barely changed with increased irradiation time (data not shown). $Ag/Ag_3PO_4/BiPO_4$ is clearly more photocatalytically active (>99% degradation within 20 min visible light irradiation) than pure $BiPO_4$ (99% degradation within 35 min UV light irradiation). When the photocatalytic degradation of MB was modeled as a pseudo–first order reaction, the rate constant for degradation by $Ag/Ag_3PO_4/BiPO_4$ was estimated to be 0.245 min^{-1}, over twice the equivalent rate constant for $BiPO_4$ (0.121 min^{-1}), as indicated by the data in Figure 3B.

3.4 Photocatalytic disinfection

The photocatalytic antibacterial activity of $BiPO_4$ and $Ag/Ag_3PO_4/BiPO_4$ toward *E. coli* was evaluated under visible light irradiation. In the absence of the catalyst, the growth of *E. coli* continued regardless of whether it was being irradiated. Figure 4A illustrates the antibacterial activity of $BiPO_4$ and $Ag/Ag_3PO_4/BiPO_4$ in the dark. $BiPO_4$ alone demonstrated no antibacterial activity, but $BiPO_4$ doped with Ag nanoparticles reduced the amount of *E. coli* by 70% within 40 min. Several studies have reported that antibacterial activity of Ag nanoparticles is caused by Ag^+ release [17]. The concentrations of Ag^+ released into an LB medium with and without *E. coli* present were 11.9 ± 0.8 and 8.10 ± 0.62 ppm, respectively. Because synthesis of $Ag/Ag_3PO_4/BiPO_4$ is based on a sonochemical procedure, it is possible to release Ag^+ ions from the $Ag/Ag_3PO_4/BiPO_4$ catalyst into the LB medium when no *E. coli* cells are present. Additionally, the secretions of *E. coli* during the growth stage accelerated the release of Ag^+ ions. Thus, the relative Ag^+ ion concentration increased by 46.9%, as a result of the improvement in the intrinsic antibacterial activity. Figure 4B shows the photocatalytic antibacterial activity of $BiPO_4$ and $Ag/Ag_3PO_4/BiPO_4$ under visible light irradiation. No obvious drop in *E. coli* could be observed in the presence and absence of $BiPO_4$ under visible light irradiation. This is because the photocatalytic disinfection of $BiPO_4$ cannot be activated by visible light. In the presence of $Ag/Ag_3PO_4/BiPO_4$, a significant increase in the activity could be found, with >99% of the *E. coli* eradicated within 20 min. This shows that $Ag/Ag_3PO_4/BiPO_4$ displays

visible light-enhanced disinfection. The concentration of Ag^+ ions released increased to 20.4 ± 1.1 ppm upon visible light irradiation. To assess the stability and efficiency of $Ag/Ag_3PO_4/BiPO_4$, a continual run of *E. coli* photocatalytic disinfection was performed. The antibacterial activity of $Ag/Ag_3PO_4/BiPO_4$ significantly decreased after three cycles. The fact suggests that the antibacterial activity of $Ag/Ag_3PO_4/BiPO_4$ did result from dissolved Ag^+ ions. Further study to enhance antibacterial stability of $Ag/Ag_3PO_4/BiPO_4$, such as doping Ag^+ ions, or halide, is now underway in our laboratory.

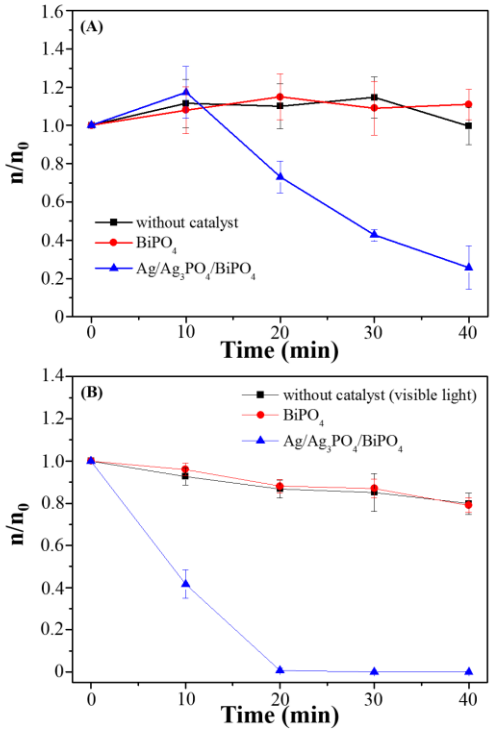

Figure 4. Concentration of *E. coli* after photocatalytic disinfection in the control, $BiPO_4$, and $Ag/Ag_3PO_4/BiPO_4$ systems (A) in the dark and (B) under visible light irradiation.

4 CONCLUSION

Ag/Ag_3PO_4 crystals deposited onto monoclinic-phase rod-like $BiPO_4$ structures were synthesized using a combination of hydrothermal and sonochemical techniques. The photocatalytic activity of the $Ag/Ag_3PO_4/BiPO_4$ heterostructure was evaluated by the degradation of MB under visible light. The evaluation results reveal that the $Ag/Ag_3PO_4/BiPO_4$ heterostructure remarkably enhanced photocatalytic activity compared with pure $BiPO_4$. This can be attributed to the high position of its VB, its high separation efficiency, and the low recombination rate of photogenerated electron–hole pairs. $Ag/Ag_3PO_4/BiPO_4$ heterostructures also displayed a light-enhanced disinfection, and this is due to hydroxyl radicals and hole production in addition to the release of Ag^+ under visible light irradiation. These strongly photocatalytic $Ag/Ag_3PO_4/BiPO_4$ heterostructures will have industrial applications for the elimination of organic pollutants and pathogens from wastewater.

ACKNOWLEDGMENTS

This study was supported by the Ministry of Science and Technology under contract (MOST 105-2113-M-018-007) and (MOST 105-2514-S-018-004).

REFERENCES

[1] R.K. Ibrahim, M. Hayyan, M.A. AlSaadi, A. Hayyan, S. Ibrahim, Environ. Sci. Pollut. Res., 23, 13754, 2016.
[2] P.H. Wang, Sep. Sci. Technol., 51, 147, 2016.
[3] L. Fernandez, V.I. Esteves, A. Cunha, R.J. Schneider, J.P.C. Tome, J. Porphyr. Phthalocyanines, 20, 150, 2016.
[4] K.M. Lee, C.W. Lai, K.S. Ngai, J.C. Juan, Water Res., 88, 428, 2016.
[5] V.M. Zainullina, V.P. Zhukov, M.A. Korotin, J. Photochem. Photobiol. C-Photochem. Rev., 22, 58, 2015.
[6] K.J. Zhu, W.Q. Yao, Y.F. Zhu, Acta Phys.-Chim. Sin., 32, 1519, 2016.
[7] Y.Y. Zhu, Q. Ling, Y.F. Liu, H. Wang, Y.F. Zhu, Appl. Catal. B-Environ., 187, 204, 2016.
[8] L. Liu, L. Ding, W.J. An, S.L. Lin, J.S. Hu, Y.H. Liang, W.Q. Cui, RSC Adv., 6, 29202, 2016.
[9] D.M. Chen, Z. Kuang, Q. Zhu, Y. Du, H.L. Zhu, Mater. Res. Bull., 66, 262, 2015.
[10] H.C. Ma, G.L. Yang, Y.H. Fu, C. Ma, X.L. Dong, X.F. Zhang, J. Chem. Eng. Jpn., 49, 366, 2016.
[11] N. Mohaghegh, E. Rahimi, Solid State Sci., 56, 10, 2016.
[12] T.-Y. Huang, Y.-J. Chen, C.-Y. Lai, Y.-W. Lin, RSC Adv., 5, 43854, 2015.
[13] H.L. Lin, H.F. Ye, B.Y. Xu, J. Cao, S.F. Chen, Catal. Commun., 37, 55, 2013.
[14] N. Ma, Y.W. Qiu, Y.C. Zhang, H.Y. Liu, Y.N. Yang, J.W. Wang, X.Y. Li, C. Cui, J. Alloy. Compd., 648, 818, 2015.
[15] L.-W. Cheng, J.-C. Tsai, T.-Y. Huang, C.-W. Huang, B. Unnikrishnan, Y.-W. Lin, Mater. Res. Express, 1, 1025023, 2014.
[16] J.Q. Li, H. Yuan, Z.F. Zhu, J. Colloid Interface Sci., 462, 382, 2016.
[17] M. Ratti, J.J. Naddeo, Y.Y. Tan, J.C. Griepenburg, J. Tomko, C. Trout, S.M. O'Malley, D.M. Bubb, E.A. Klein, Appl. Phys. A-Mater. Sci. Process., 122, 346, 2016.